Wideband Direct Detection Constraints on Hidden Photon Dark Matter with the QUALIPHIDE Experiment

K. Ramanathan,[1,*] N. Klimovich,[1,†] R. Basu Thakur,[1] B. H. Eom,[2] H. G. Leduc,[2] S. Shu,[1] A. D. Beyer,[2] and P. K. Day[2]

[1]Division of Physics, Mathematics and Astronomy, California Institute of Technology, Pasadena, California 91125, USA
[2]Jet Propulsion Laboratory, California Institute of Technology, Pasadena, California 91109, USA

(Received 17 September 2022; revised 27 March 2023; accepted 5 May 2023; published 9 June 2023)

We report direction detection constraints on the presence of hidden photon dark matter with masses between 20–30 $\mu\mathrm{eV\,c^{-2}}$, using a cryogenic emitter-receiver-amplifier spectroscopy setup designed as the first iteration of QUALIPHIDE (quantum limited photons in the dark experiment). A metallic dish sources conversion photons, from hidden photon kinetic mixing, onto a horn antenna which is coupled to a *C* band kinetic inductance traveling wave parametric amplifier, providing for near quantum-limited noise performance. We demonstrate a first probing of the kinetic mixing parameter χ to the 10^{-12} level for the majority of hidden photon masses in this region. These results not only represent stringent constraints on new dark matter parameter space, but are also the first demonstrated use of *wideband* quantum-limited amplification for astroparticle applications.

DOI: 10.1103/PhysRevLett.130.231001

The nature of dark matter (DM) remains elusive, with an enormous available mass parameter space for potential particle physics candidates to occupy—stretching from 10^{-22} $\mathrm{eV\,c^{-2}}$ ultralight particles to many solar-mass black holes. Recent astroparticle community reports stress the need for experiments to look throughout this parameter space and, crucially, develop techniques to do so efficiently [1]. If the dark matter is very light, with a number density per wavelength volume $\gg 1$, this suggests strategies that can exploit the resultant wavelike nature of the dark matter. The classic example in this regime is the axion, which can be searched for by its coupling with electromagnetism and subsequent conversion to an ordinary photon [2]. Hidden photons, massive vector bosons also known in the literature as dark photons, are another well-motivated candidate in this vein [3]. The relevant Lagrangian terms for these,

$$\mathcal{L} \supset \frac{m_\gamma^2}{2} X_\mu X^\mu - \frac{\chi}{2} F_{\mu\nu} X^{\mu\nu}, \tag{1}$$

show the key feature of this model, a "mixing" of the visible and hidden photon with kinetic mixing parameter χ. Here $F_{\mu\nu}$ is the field strength of electromagnetism and $X_{\mu\nu}$ is the hidden counterpart, for a hidden photon (X_μ) of mass m_γ. Hidden photons, arising from a diverse set of beyond the standard model theories (see Ref. [4] for comprehensive reviews), have attracted attention in the previous decade because they are a benchmark model that can plausibly be the entirety of the DM or act as a mediator themselves to an entire dark sector, created in the early Universe through certain nonthermal means [5].

Importantly, the hidden photon kinetic mixing outlined in Eq. (1) sources a global oscillating ordinary electric field in free space. Under the assumption that hidden photons comprise the entirety of the dark matter (of local density ρ_{DM}), the average amplitude of the terrestrial E field is $\langle|\mathbf{E}_{\mathrm{DM}}|^2\rangle \propto 2\chi^2\rho_{\mathrm{DM}}$, with corresponding frequency $\nu_{\mathrm{DM}} \approx 0.24\ \mathrm{GHz}(m_\gamma/\mu\mathrm{eV})$ [6]. Remarkably then, any conducting surface with boundary condition $\mathbf{E}_{\parallel} = 0$, such as a metallic plate, will source radiation perpendicular to its surface due to dark matter conversion effects, based on the existence of $\mathbf{E}_{\mathrm{DM}}$. This idea, as first described in Ref. [6], points to a generic wideband approach of looking for excess photon power from a surface as the signature of electromagnetically coupled dark matter. A particularly simple implementation of a spherical cap of area A_d will concentrate an emission power $P_d \propto \chi^2\rho_{\mathrm{DM}}A_d$ onto its geometrical focus. Feeding this radiation at frequency ν_{DM} into an antenna-receiver setup allows one to spectroscopically search for the signature of any extant hidden photon dark matter with such a "dish haloscope" design.

For such a model of hidden photons under a fixed polarization scenario [7], coupled to a single polarization antenna at the focal point, and with a unified literature assumption of $\rho_{\mathrm{DM}} = 0.45\ \mathrm{GeV\,cm^{-3}}$ [8], the expected sensitivity for χ with a spherical dish and minimum detectable power P_{det} is

$$\chi_{\mathrm{sens}} = 6.9 \times 10^{-14} \left(\frac{P_{\mathrm{det}}}{10^{-23}\ \mathrm{W}}\right)^{1/2} \left(\frac{1\ \mathrm{m}^2}{A_d}\right)^{1/2} \epsilon_c^{-1/2} \tag{2}$$

We have introduced a coupling efficiency ϵ_c in Eq. (2) to account for signal degradation due to geometric mismatches and transmission losses. With their potentially large instantaneous bandwidth (only limited by the antenna coupling and readout electronics), this style of dark matter detection offers an alternative to resonant cavity hidden photon searches done by ADMX, HAYSTAC, and other experiments [9,10]. In addition, dish searches can explore axion parameter space with the addition of a magnetic field, leveraging a similar Primakoff conversion mechanism as cavity experiments [2]. Such schemes are already hotly pursued research and development efforts [11,12].

In this Letter, we present results from the first iteration of QUALIPHIDE (quantum limited photons in the dark experiment), a dish haloscope search for hidden photons in the C band (roughly 4–8 GHz) that focuses on improved sensitivity in this regime as compared to prior literature efforts [13,14].

In the language of radiometry, the signal-to-noise ratio of any excess power measurement can be expressed as $\mathrm{SNR} = (P_d/k_B T_{\mathrm{syst}})\sqrt{\tau/\Delta}$ for a measurement bandwidth Δ, system noise temperature T_{syst}, and exposure time τ. Given fixed measurement parameters then, there are two obvious ways one can improve experimental sensitivity: increasing P_{em} or decreasing T_{syst} (i.e., improving the minimum detectable power). The former is most easily achieved by increasing the emission area, an approach taken by experiments such as Refs. [13,14] with large $A_d \sim \mathrm{m}^2$ dishes kept at room temperature. Despite this progress, a substantial amount of χ-m_γ parameter space remains unexplored, particularly at microwave frequencies $\nu_{\mathrm{DM}} > 7$ GHz, where there is a notable weakening of astrophysical and cosmological measurements limits [15]. QUALIPHIDE takes the alternative approach of dropping T_{syst} down close to the standard quantum limit (SQL). The SQL, as outlined in the seminal work of Ref. [16], is a statement of having unavoidable noise from two sources: zero-point vacuum fluctuations, and that any phase-insensitive signal amplification process must respect an underlying quantum mechanical uncertainty principle. Together these add *at least* one quanta [17] of noise to the measurement. QUALIPHIDE achieves near SQL performance ($T_{\mathrm{syst}} \gtrapprox h\nu_{\mathrm{DM}}/k_B$) by placing the setup into a 20 mK environment, a logical extension of prior ~3 K experiments like Refs. [13,16], and feeding the output to a traveling-wave kinetic inductance parametric amplifier (TWKIPA).

TWKIPAs are state-of-the-art superconducting NbTiN devices with demonstrated 20 dB gain over an octave or more of bandwidth at gigahertz frequencies, with design and operation details as laid out in Ref. [18]. Briefly, the amplifier is able to take an input pump tone of frequency ν_p and transfer power to an input signal tone of frequency ν_s, subsequently generating an amplified output signal along with an "idler" tone at $\nu_i = \nu_p - \nu_s$, with a signal gain of G_{pa}.

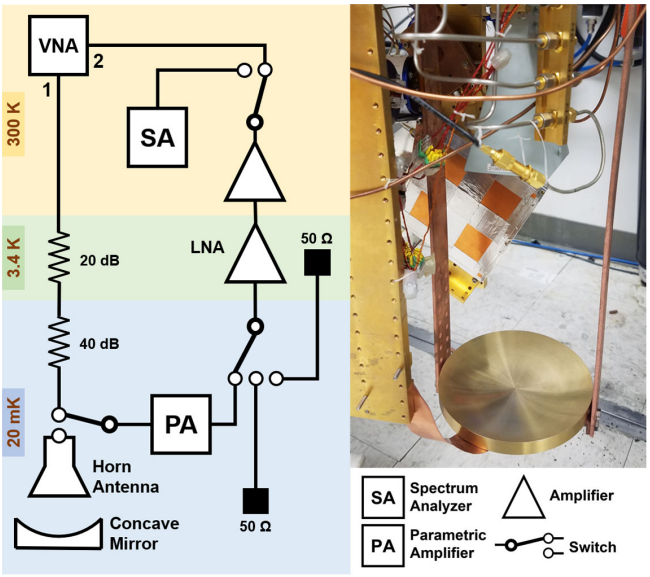

FIG. 1. Left: schematic of a simplified version of the cryogenic-to-room-temperature experimental layout, as described in text. Right: photograph of the QUALIPHIDE setup showing the mK stage dish, support, and antenna components.

Figure 1 shows a photograph (right) and simplified schematic (left) of the QUALIPHIDE setup. A 12.7-cm-diameter gold-plated copper dish ($A_d = 0.0127\ \mathrm{m}^2$) is used, chosen for its low thermal emissivity of $\varepsilon_s \approx 2 \times 10^{-3}$ [19], and manufactured to $\mathcal{O}$ (mm) precision. It is attached using a copper frame and pointed to a 4.75–11 GHz commercial single polarization horn antenna (AINFO LB-475110-10-C-SF) placed 22 cm away at the antenna phase center. The entire structure is mounted to the final mK stage of a Leiden dilution refrigerator to minimize the thermal background. We calculate the background radiation noise equivalent power for the setup to be $2 \times 10^{-23}\ \mathrm{W}/\sqrt{\mathrm{Hz}}$ [20]. The antenna is routed to the TWKIPA, with associated circuitry for introducing and dumping the pump tone and dc current [18], after which it is amplified by a commercial low noise amplifier (LNA, Low Noise Factory LNC0.3_14B, $T_{\mathrm{noise}} \sim 3$ K) and further room temperature amplification, before being sent either to a Vector Network Analyzer (VNA) or Signal Hound SM200B spectrum analyzer. A cold switch before the input of the parametric amplifier allows for the incident signal to be switched between the antenna-dish setup and 20 mK load used for reference data. A second cold switch immediately following the parametric amplifier connects to both a "hot" 3.38 K and "cold" 20 mK load used for calibrating the system noise via a y-factor measurement.

The dish area, choice of antenna location, and single run configuration were limited by available space and time in the refrigerator as the measurement was conducted parasitically to existing experiments. The signal at this frequency and configuration is expected to form a convergent

spherical wave with a circular focal spot [6,14]. However, due to expected diffraction effects among other concerns (see Appendix A for details), we include a frequency-dependent coupling efficiency of $\epsilon_c \sim 0.3$. Angular shifts of the signal due to dark matter velocity dispersion effects are considered but are calculated to introduce only negligible deviations of $\ll 1\%$ [6].

Our experimental procedure involves four spectrum analyzer measurements: the power emitted by the dish P_{d}, the power emitted by the reference load P_{ref}, and the power emitted by the hot and cold loads after the parametric amplifier (P_H and P_C). The latter three measurements combined with G_{pa} allow us to refer the spectrum analyzer noise level to the number of noise quanta at the input of the parametric amplifier (N_{pa}) in a y-factor measurement as described in Ref. [18]. The overall system noise is dominated by the first amplifier(s) in the readout chain because the amplified noise contribution of the first amplifier greatly exceeds the noise contributions of the subsequent amplifiers. In our case this is well approximated by $N_{\mathrm{syst}} = N_{\mathrm{pa}} + N_{\mathrm{LNA}}/(G_{\mathrm{pa}}A)$. The attenuation A between the parametric amplifier and LNA is based on measured S_{21} transmission reference data for individual components and is taken to be a conservative estimate of -4 dB in this analysis. The frequency-dependent LNA noise is extracted from its data sheet. The noise result across frequencies is shown in Fig. 2, with the more than 20 dB gain of the amplifier shown in the inset, which makes it the dominant contribution to the system noise in the regions where it has high gain. The large-scale structures visible in this result stem from the impedance linked ripples of both the TWKIPA operation as well as in switching the cold switch between hot load, cold load, and amplifier channels. Using the calculated value directly would occasionally result in the unphysical choice of $N_{\mathrm{syst}} < 1$, which as discussed earlier is a fundamental bound from the theory of phase-insensitive linear amplification [16]. As a result, we instead choose a conservative 95th-percentile upper bound, the dashed line in the figure, of $N_{\mathrm{syst}} \approx 2.1$.

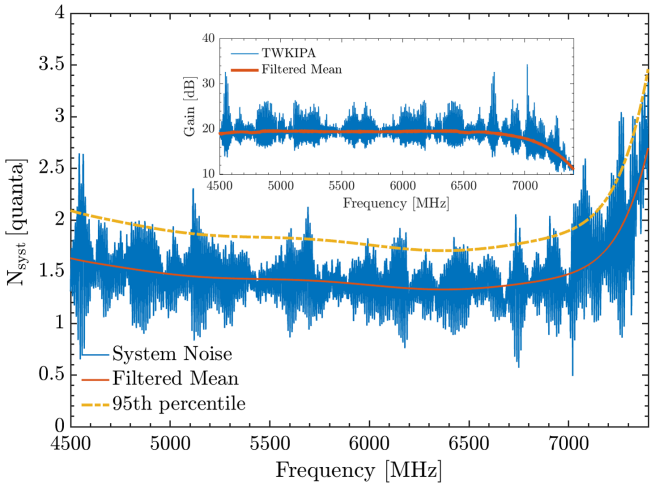

FIG. 2. The overall system noise with 95th-percentile upper bound (yellow dashed line), referred to the input of the parametric amplifier. Inset: gain of the TWKIPA in the frequency regime of the experiment.

Next, we integrate the signal emitted by both the dish and reference load for 8.27 h each. This sweep is performed in 160 MHz instantaneous bandwidth steps from 3.9 to 7.4 GHz, which covers the region where the parametric amplifier provides > 15 dB of gain, with resultant datasets as seen in Fig. 3, bottom left. The spectrum analyzer was configured to use a flattop window function with a resolution bandwidth of 3 kHz and video bandwidth of 3 Hz, providing for an instrument preset bin size of $\Delta_b = 762$ Hz. These choices reflect a balance between maximizing the SNR of the signal by matching the expected frequency dispersion of the dark matter [$\delta\nu \approx 10^{-6}\nu$, $\mathcal{O}$ (kHz)], due to the relative velocity of the galactic dark matter halo, and the bandwidth limited readout speed of the analyzer.

Switching the system input cold switch causes an additional shift of the ripple structure due to the altered path length for the standing wave reflections in the setup and the differential between the 377 Ω free-space impedance and 50 Ω rf components. We also see a broadband ∼0.4 dB excess in the dish spectrum, attributed to environmental emission picked up by the antenna. In conjunction, these differences create a frequency-dependent offset in the residual, as seen in Fig. 3, right, between the dish data and reference that must be modeled. We compensate for these effects with a method similar to that used by cavity experiments [9]—applying a combination of smoothing filters that removes the large megahertz-scale residual variations caused by the aforementioned effects while preserving the kilohertz-scale structure (see Appendix A for further details about this filtering process).

The resulting residual, found to be Gaussian over 10 MHz windows, is seen in Fig. 3, top left, and shows that fluctuations in the measurement have been averaged to ∼0.01 quanta at the input of the parametric amplifier. We exclude two data regions in the dish dataset with large noise features, at 5.19–5.21 GHz (and its idler), traced to the existence and use of WiFi channel 40 [21] in the lab. Prior to analysis, we then sum the power of each neighboring set of five bins to effectively decorrelate the spectrum analyzer effect of using overlapping windows on the order of the flattop width [9,13].

We use a literature standard isothermal Maxwellian dark matter velocity distribution with escape velocity $v_{\mathrm{esc}} = 544\ \mathrm{km\,s^{-1}}$, mean $v_0 = 220\ \mathrm{km\,s^{-1}}$, and periodic Earth motion with velocity $v_E = 232\ \mathrm{km\,s^{-1}}$. The velocity profile introduced frequency dispersion results in a relation between hidden photon frequency and dark matter velocity v of $h\nu_{\mathrm{DM}} = m_\gamma c^2/\sqrt{1-(v/c)^2}$. We do not modify the dark matter distribution due to any terrestrial electromagnetic shielding as the probed χ is $\ll 1$ and is thus incredibly

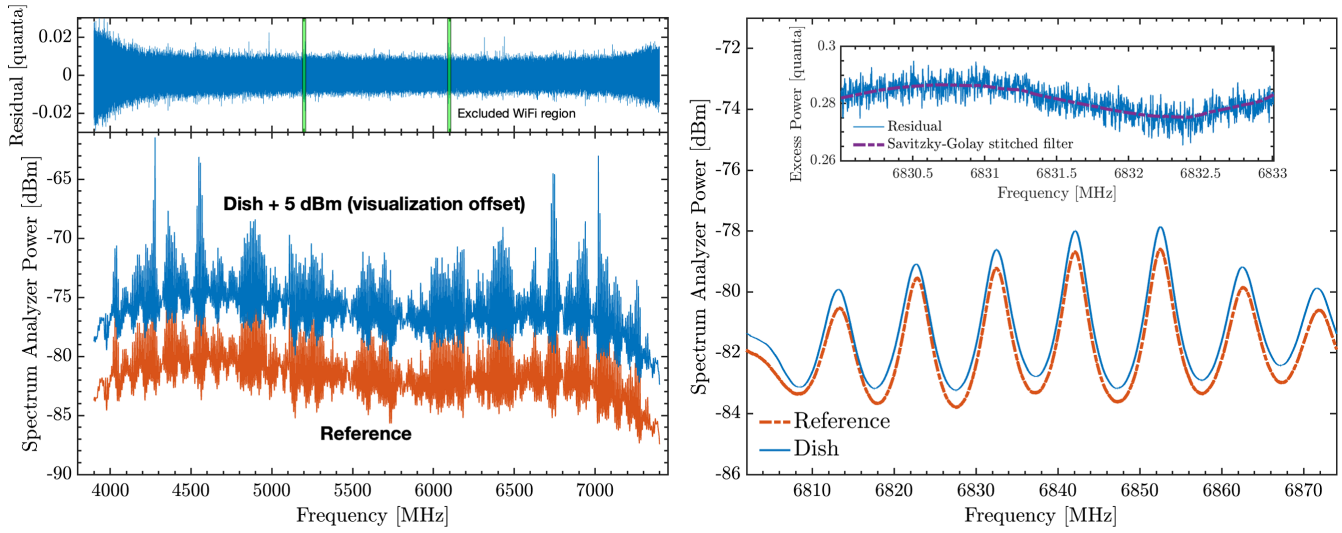

FIG. 3. Bottom left: integrated reference and dish data (offset by +5 dBm for visualization purposes) taken over the 8 h exposure. Right: enlargement of the 6.84 GHz region, showing both the impedance mismatch ripple structure and excess broadband power present in the dish data. Right-hand inset: residual of the dish and reference, showing the ripple mismatch between datasets, which introduces further sinusoidal structure. Dashed (purple) line is the Savitzky-Golay filter, as described in the text, used to compensate for these effects. Top left: the final filtered residual over the 3.5 GHz region of interest, with green band regions excluded from the analysis due to WiFi interference effects.

weakly shielded (which goes as χ^2 by a similar argument to dish emission).

Constraining the signal power is then done through a likelihood analysis in (χ, m_γ) space. We generate a signal and idler model for a given frequency $\nu_{\rm DM}$, stepping through the data in $\delta\nu_{\rm DM} \sim 10$ kHz intervals, which are then convolved with an experimentally measured flattop spectrum analyzer response to a single frequency tone. The fitting range is set at $[\nu_{\rm DM} - 25\ {\rm kHz}, \nu_{\rm DM} + 75\ {\rm kHz}]$ and mirrored for the idler. An example of the expected spectral shape can be seen in Fig. 4, for a simulated signal injected into the raw dataset around 4 GHz, chosen because no signal mode will be supported by the antenna at that frequency. Notably, a mirrored version of the signal with an amplitude scaling of $1 - 1/G_{\rm pa}$ should also appear at the parametric amplifier idler frequency as a result of the amplification process; see Fig. 4 inset. Because this ratio is near unity, any dark matter signal will effectively appear twice within the measurement, doubling the integration time in terms of its signal-to-noise ratio. The combined signal and idler model is used to search for excesses as a function of χ within the data according to the expected power given by Eq. (2), using a standard Gaussian log-likelihood formalism. We determine no presence of a hidden photon dark matter signal (see Appendix B for complete analysis details). Next, we compute the confidence limits by way of a likelihood-ratio test with resulting 95% confidence limits on χ from QUALIPHIDE, as shown in Fig. 5. The limit can be directly compared to those shown from cavity haloscopes [9] and other dish experiments [14], due to their reinterpretation by Ref. [8] to have consistent $\rho_{\rm DM}$ under a fixed polarization scenario. We note the characteristic narrow but deep limits set by cavity experiments, indicative of their resonant enhancement trade-off with scan time. Conversely, as QUALIPHIDE is able to demonstrate, dish experiments can explore large chunks of parameter space to within an order of magnitude sensitivity even with $\mathcal{O}$ (min) exposures using an undersized $\mathcal{O}$ (100) cm^2 dish relative to the cryostat volume. Details of the systematic checks done to ensure the robustness of the result can be found in Appendix B.

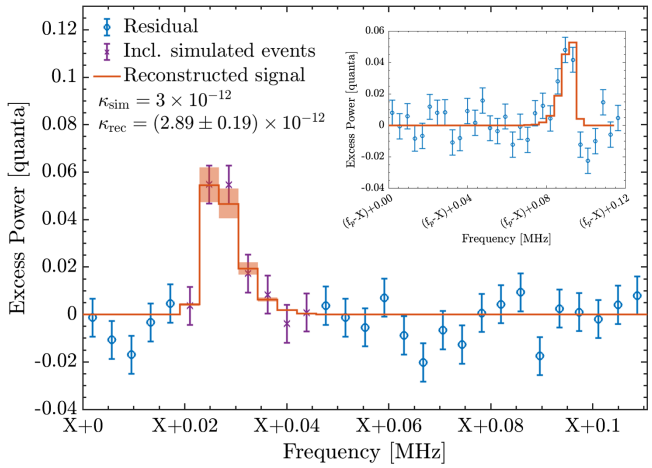

FIG. 4. Example of a signal at $\nu_{\rm DM} = 7$ GHz with $\chi = 3 \times 10^{-12}$, injected into a data window around 4 GHz, and overlaid with the signal reconstruction. Inset: corresponding idler location and resultant fit.

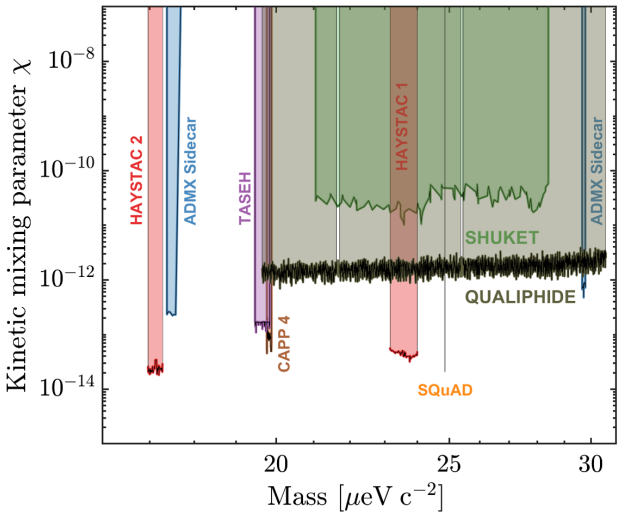

FIG. 5. 95% confidence limits (gray) on the kinetic mixing parameter χ as obtained by QUALIPHIDE (with WiFi cut-out regions) overlaid with reinterpreted limits from the ADMX, HAYSTAC, CAPP, SQuAD, and TASEH cavity experiment families [9,10] along with the SHUKET dish experiment [14]. Reinterpreted data taken from Ref. [8].

In summary, we have conducted a search for hidden photon dark matter and found no presence of a signal for most masses in the range between $[1.97, 3.05]\times 10^{-5}$ eV c^{-2}, excluding a kinetic mixing parameter χ at the 95% confidence level to extremal values of $[0.79, 3.81]\times 10^{-12}$ across that frequency range. This result represents the first use of wideband quantum-limited amplification to hunt for dark matter and indicates that quantum-limited dish experiments are a fruitful avenue for future searches. Finally, the forthcoming availability of K to W band TWKIPAs [22] and the addition of a magnetic field will allow for the next evolution of QUALIPHIDE to look for theoretically very well motivated postinflationary axion dark matter at $\sim$65 μeV c^{-2} [23].

We would like to thank Sunil Golwala for useful conversations relating to light dark matter searches. The research was carried out at the Jet Propulsion Laboratory, California Institute of Technology, under a contract with the National Aeronautics and Space Administration (80NM0018D0004). K. R. is supported by the Troesh family fellowship at the California Institute of Technology.

Appendix A: Data processing.—Coupling efficiency: ϵ_c consists of three multiplicative coefficients to model any frequency-dependent antenna-dish mismatch. The first term, between 0.79–0.84 in the frequency regime of interest, accounts for imperfect power coupling and is numerically computed from an overlap integral between the focal pattern and the antenna gain pattern taken from the manufacturer data sheet, using a Gaussian beam analysis like in Refs. [14,23]. Next, ϵ_c includes an attenuation term of 0.39 (−4 dB) to account for signal degradation (between antenna and TWKIPA) due to the placement of passive circuit components. Finally, we estimate the angular deviation of the dish with respect to the antenna as within 2° of vertical, which introduces a 5% systematic into ϵ_c. We use a simplified COMSOL5.5 simulation of the dish and antenna setup to validate the constrained geometry and verify the expected signal coupling to within 20% across the measurement band.

Filtering: Switching from the hot and cold loads to the mirror results in large-scale frequency-dependent structures within the raw transmission residual between those two datasets due to the change in the internal reflections within the system. This structure contains several megahertz-scale variations along with several hundred kilohertz-scale peaks where the ripple structure of the TWKIPA has slightly shifted. We apply a combination of two third-order Savitzky-Golay filters with a 2.5 MHz and 250 kHz window to remove features within the residual broader than 1 MHz and 100 kHz, respectively. While the smaller window is necessary for fitting the peaks of the slightly shifted ripple structure, it results in overfitting of flatter regions that are well modeled by the larger window smoothing filter. To circumvent this concern, we smoothly stitch together both fits using a weighted average with weights $(w_2/w_1)^2$ and $1-(w_2/w_1)^2$, where $w_{1,2}$ is the sum of the residual over a 500 kHz Blackman-Harris window centered at each data point for the fit. This combination favors the large-window fit while smoothly transitioning to the smaller window in near peak regions where the former fails to properly match the structures in the data.

Amplifier gain: The gain of the parametric amplifier was only recorded above 4.5 GHz so we use the mirror image of the corresponding idler gain above $f_p/2$ for the frequencies below it. In the 1.15 GHz range where the data are present, this estimate agrees to within a mean absolute deviation of 0.05 dB and is dominated by the excess in our estimate of A.

Appendix B: Data analysis.—Likelihood analysis: The analysis starts with the binned Gaussian negative log-likelihood$\mathcal{LL}$ function,

$$\mathcal{LL} = \sum_{k=S,I}\sum_{i=1}^{n}\log(\sigma_{k,i}^2) + \frac{1}{\sigma_{k,i}^2}(P_{k,i}^{\text{model}} - P_{k,i}),$$
$$\text{with}\quad \sigma_{k,i}^2 = \sigma_{\text{white}}^2 + \sigma_{\text{em}}^2 + N_{k,i}, \tag{B1}$$

per bin signal and idler power $P_{k,i}$, model power $P_{k,i}^{\text{model}}$ [derived from Eq. (2)], and bin error terms $\sigma_{k,i}$. The latter is composed of a *white* noise term estimated from two neighboring nonoverlapping fit windows, a thermal emission (em) term due to broadband subtraction of the reference from the dish, and a per bin shot noise term $N_{k,i} \equiv b_{k,i}\cdot P_{k,i}^{\text{model}}\tau/(h\nu_{\text{DM}})$, based on the expected signal

weight $b_{k,i}$ and exposure time τ, accounting for very weak signals from small χ.

The minima are consistent with a nonzero signal (i.e., local "p values" of $\sim 10^{-4}$) for certain masses. However, we account for the look-elsewhere effect with the methodology from Ref. [24], where using the Monte Carlo method we determine the number of independent frequency windows ($\gtrapprox 10^5$) in the sample and reevaluate the discovery significance. This drops the excess in any bin below $\sim 1\sigma$ significance, implying no evidence of hidden photons. The 95% confidence limits are computed from the test statistic $\Lambda = 2(\mathcal{LL}_{\rm model} - \mathcal{LL}_{\rm min})$. We verify that Λ is $\chi^2_{1\,\rm d.o.f.}$ distributed as expected via a Monte Carlo simulation of 1000 injected and reconstructed signals each for a set of 10 randomly chosen $\nu_{\rm DM}$ spanning the search space.

Systematic checks: Select checks are performed to ensure robustness of the results. To ensure that the data cleaning process did not bias any reconstruction, we use a Monte Carlo simulation to inject 1000 signals of χ between $0.7\text{–}4 \times 10^{-12}$ and $\nu_{\rm DM}$ between 4–8 GHz into a 100 MHz window around the 4 GHz region and verify accurate reconstruction of χ, an example of which is again shown by Fig. 4 in the main text. We modify the Savitzky-Golay filter parameters (order$^{+2}_{-1}$ and frequencies $\pm 10\%$), which change χ limits at the 10% level. Systematics in the received power arising from polarization offsets, and changes in the power coupling from effects like dish-antenna misalignment, frequency-dependent antenna gain, and diffraction effects, can all be modeled through changes in ϵ_c and are seen to follow the expected $P_{\rm det} \propto \chi^2$ relation at the output of the analysis.

*karthikr@caltech.edu
†nikita@alumni.caltech.edu

[1] M. Battaglieri *et al.*, arXiv:1707.04591, and references therein; R. Kolb *et al.*, Basic Research Needs for Dark-Matter Small Projects New Initiatives: Report of the Department of Energy's High Energy Physics Workshop on Dark Matter, 10.2172/1659757.

[2] P. Sikivie, Phys. Rev. Lett. **51**, 1415 (1983); G. G. Raffelt, Astrophysical axion bounds, in *Axions: Theory, Cosmology, and Experimental Searches*, edited by M. Kuster, G. Raffelt, and B. Beltrán (Springer, Berlin, 2008), pp. 51–71.

[3] L. B. Okun, Zh. Eksp. Teor. Fiz. **83**, 892 (1982) [Sov. Phys. JETP **56**, 502 (1982)]; B. Holdom, Phys. Lett. **166B**, 196 (1986).

[4] J. Jaeckel and A. Ringwald, Annu. Rev. Nucl. Part. Sci. **60**, 405 (2010); P. W. Graham, J. Mardon, and S. Rajendran, Phys. Rev. D **93**, 103520 (2016).

[5] P. Arias, D. Cadamuro, M. Goodsell, J. Jaeckel, J. Redondo, and A. Ringwald, J. Cosmol. Astropart. Phys. 06 (2012) 013; A. E. Nelson and J. Scholtz, Phys. Rev. D **84**, 103501 (2011); J. Redondo and M. Postma, J. Cosmol. Astropart. Phys. 02 (2009) 005; A. Filippi and M. De Napoli, Rev. Phys. **5**, 100042 (2020).

[6] D. Horns, J. Jaeckel, A. Lindner, A. Lobanov, J. Redondo, and A. Ringwald, J. Cosmol. Astropart. Phys. 04 (2013) 016; J. Jaeckel and J. Redondo, J. Cosmol. Astropart. Phys. 11 (2013) 016; J. Jaeckel and S. Knirck, J. Cosmol. Astropart. Phys. 01 (2016) 005.

[7] To be precise, a zenith-facing dish located at 35° latitude implying an averaged polarization term $\langle \alpha^2 \rangle \approx 0.38$ in the underlying model of Ref. [6].

[8] A. Caputo, A. J. Millar, C. A. J. O'Hare, and E. Vitagliano, Phys. Rev. D **104**, 095029 (2021); C. O'Hare, cajohare/axionlimits: Axionlimits (2020), 10.5281/zenodo.3932430.

[9] S. J. Asztalos *et al.*, Phys. Rev. Lett. **104**, 041301 (2010); L. Zhong *et al.*, Phys. Rev. D **97**, 092001 (2018); A. V. Dixit, S. Chakram, K. He, A. Agrawal, R. K. Naik, D. I. Schuster, and A. Chou, Phys. Rev. Lett. **126**, 141302 (2021); H. Chang *et al.* (TASEH Collaboration), Phys. Rev. Lett. **129**, 111802 (2022); C. Boutan *et al.* (ADMX Collaboration), Phys. Rev. Lett. **121**, 261302 (2018); Y. Lee, B. Yang, H. Yoon, M. Ahn, H. Park, B. Min, D. L. Kim, and J. Yoo, Phys. Rev. Lett. **128**, 241805 (2022).

[10] K. M. Backes, D. A. Palken, S. A. Kenany, B. M. Brubaker, S. Cahn, A. Droster, G. C. Hilton, S. Ghosh, H. Jackson, S. K. Lamoreaux *et al.*, Nature (London) **590**, 238 (2021).

[11] J. Egge, S. Knirck, B. Majorovits, C. Moore, and O. Reimann, Eur. Phys. J. C **80**, 1 (2020).

[12] J. Liu *et al.* (BREAD Collaboration), Phys. Rev. Lett. **128**, 131801 (2022).

[13] N. Tomita, S. Oguri, Y. Inoue, M. Minowa, T. Nagasaki, J. Suzuki, and O. Tajima, J. Cosmol. Astropart. Phys. 09 (2020) 012.

[14] P. Brun, L. Chevalier, and C. Flouzat, Phys. Rev. Lett. **122**, 201801 (2019); J. Suzuki, T. Horie, Y. Inoue, and M. Minowa, J. Cosmol. Astropart. Phys. 09 (2015) 042; A. Andrianavalomahefa *et al.* (The FUNK Experiment Collaboration), Phys. Rev. D **102**, 042001 (2020); S. Knirck, T. Yamazaki, Y. Okesaku, S. Asai, T. Idehara, and T. Inada, J. Cosmol. Astropart. Phys. 11 (2018) 031.

[15] A. Mirizzi, J. Redondo, and G. Sigl, J. Cosmol. Astropart. Phys. 03 (2009) 026; H. An, M. Pospelov, and J. Pradler, Phys. Lett. B **725**, 190 (2013); S. D. McDermott and S. J. Witte, Phys. Rev. D **101**, 063030 (2020).

[16] C. M. Caves, Phys. Rev. D **26**, 1817 (1982); S. Kotaka, S. Adachi, R. Fujinaka, S. Honda, H. Nakata, Y. Seino, Y. Sueno, T. Sumida, J. Suzuki, O. Tajima, and S. Takeichi (DOSUE-RR Collaboration), Phys. Rev. Lett. **130**, 071805 (2023).

[17] $h\nu$ per second per hertz of bandwidth.

[18] N. S. Klimovich, Traveling wave parametric amplifiers and other nonlinear kinetic inductance devices, Ph.D. thesis, California Institute of Technology, 2022; B. Ho Eom, P. K. Day, H. G. LeDuc, and J. Zmuidzinas, Nat. Phys. **8**, 623 (2012).

[19] J. J. Bock, M. K. Parikh, M. L. Fischer, and A. E. Lange, Appl. Opt. **34**, 4812 (1995).

[20] D. Benford, T. Hunter, and T. G. Phillips, Int. J. IR & mm Waves **19**, 931 (1998).
[21] IEEE Computer Society LAN/MAN Standards Committee and others, IEEE Std 802.11-2020, 1 (2021), https://standards.ieee.org/ieee/802.11/7028/.
[22] G. Che *et al.*, arXiv:1710.11335.
[23] M. Buschmann, J. W. Foster, A. Hook, A. Peterson, D. E. Willcox, W. Zhang, and B. R. Safdi, Nat. Commun. **13**, 1 (2022); P. F. Goldsmith, *Quasioptical Systems*, IEEE Press Series on RF & Microwave Technology (IEEE Publications, New York, 1997).
[24] J. W. Foster, N. L. Rodd, and B. R. Safdi, Phys. Rev. D **97**, 123006 (2018).